Carbohydrate Polymer Technologies and Applications 8 (2024) 100564

Contents lists available at ScienceDirect

Carbohydrate Polymer Technologies and Applications

journal homepage: www.sciencedirect.com/journal/carbohydrate-polymer-technologies-and-applications

Antibacterial nanofibrous wound dressing mats made from blended chitosan-copper complexes and polyvinyl alcohol (PVA) using electrospinning

Amir Parvinnasab [a,1], Sharareh Shahroudi [a,1], Erfan Salahinejad [a,*], Amir Hossein Taghvaei [b], Seyed Adel Sharifi Fard [c], Esmaeel Sharifi [d]

[a] Faculty of Materials Science and Engineering, K. N. Toosi University of Technology, Tehran, Iran
[b] Department of Materials Science and Engineering, Shiraz University of Technology, Shiraz, Iran
[c] Student Research Committee, Hamadan University of Medical Science, Hamadan, Iran
[d] Department of Tissue Engineering and Biomaterials, School of Advanced Medical Sciences and Technologies, Hamadan University of Medical Sciences, Hamadan, Iran

ARTICLE INFO

Keywords:
Wound dressings
Chitosan-copper complexes
Electrospinning
Biocompatibility
Antibacterial
Wound healing

ABSTRACT

Chitosan is promising for wound care solutions owing to its high biocompatibility, biodegradability, hemostasis, antimicrobial activity, and promotion of tissue regeneration. However, its antibacterial property is insufficient for some infected wounds and local conditions. Given the high antibacterial activity of copper, this work focused on synthesizing chitosan-copper complexes with 1, 3, 6, 12, 24, and 48 % copper to chitosan's amine groups, followed by electrospinning them with polyvinyl alcohol. The mats exhibited promising vapor transition rates ranging from 2800 ± 33 to 3201 ± 48 g/m2.day and a dual-phase release of copper, with an initial burst followed by a sustained release over 7 days. Superior fibroblast cell cytocompatibility was observed up to 12 % copper, with accelerated re-epithelialization and cell migration to 6 % copper. Antibacterial efficacy against both gram-positive *Staphylococcus aureus*)*S. aureus*(and gram-negative *Escherichia coli* (*E. coli*) bacteria was effective beyond 3 % copper. Typically, the optimal concentration of copper was identified at 6 %, exhibiting a balance of antibacterial activity and biocompatibility, with the ability to cover 98.0 ± 0.8 % of the wound area in only 24 h and increase cell proliferation by 189 ± 11 % within 5 days.

1. Introduction

The skin accounts for approximately eight percent of the body's weight and serves as the first defensive line of the body. Skin wounds pose a significant challenge in the realm of medical care due to their prevalence and diverse causes (Percival, 2002; Beam, 2007). Skin wounds, especially open ones, are highly susceptible to infections and the overuse of antibiotics to treat this issue has detrimental impacts on both the environment and human health. As a prevailing global issue, there is a growing exploration of novel alternatives aimed at mitigating disease prevalence and minimizing adverse health consequences.

Recent advancements in science and technology have paved the way for an extensive range of materials and routes for fabricating wound dressings. Commonly used materials in this filed include cellulose, collagen, gelatin, chitosan, hyaluronic acid, silk fibroin, polyurethane, polyethylene glycol (PEG), poly(lactic-co-glycolic acid) (PLGA), and polycaprolactone (PCL). Among them, chitosan is particularly distinct due to its unique combination of biocompatibility, hemostatic properties, antimicrobial activity, wound healing, tissue regeneration, chelating capacity, and cost-effectiveness (Yilmaz Atay, 2019; Feng et al., 2021; Yang et al., 2022). Chitosan is derived from chitin through a process called deacetylation, with chitin found in the exoskeletons of crustaceans like shrimp and crabs, as well as in the cell walls of fungi. Specifically, the intrinsic antibacterial property of chitosan is owing to interactions between its positively-charged amino groups and anionic groups existing in gram-positive bacteria's lipoteichoic acids or gram-negative bacteria's lipopolysaccharides (Kong et al., 2010; Rabea et al., 2003). While chitosan is a promising antimicrobial agent (effective against bacteria, viruses, fungi, and parasites), its effectiveness can vary based on its grade, wound type, and local conditions. The grade of

* Corresponding author.
E-mail address: salahinejad@kntu.ac.ir (E. Salahinejad).
[1] These authors contributed equally and share co-first authorship.

https://doi.org/10.1016/j.carpta.2024.100564

Available online 2 September 2024

chitosan, determined by its degree of deacetylation and molecular weight, significantly impacts its antimicrobial efficacy, with lower molecular weight and higher deacetylation enhancing effectiveness. Chitosan is generally more effective in acute wounds, but its efficacy may be reduced in chronic or infected wounds due to complex microbial environments. Moisture levels, pH, and the presence of proteases or biofilms can impact chitosan's antibacterial effectiveness, with optimal performance occurring in acidic, moderately moist conditions free from excessive bacterial protection (Verlee et al., 2017; Li & Zhuang, 2020). Accordingly, to achieve optimal broad-spectrum antibacterial results, it is necessary to combine chitosan with other antimicrobial substances or treatments.

Copper (Cu) has a significant antibacterial effect that can help overcome the antibacterial limitations of chitosan. It also functions as a cofactor for some metalloproteinases and enzymes. Human endothelial cells, growth factors, and hypoxia-inducible factor (HIF-1) are all stimulated by Cu, which results in the development of new blood vessels (Mroczek-Sosnowska et al., 2015; Li et al., 2012). There are both chemical and physical methods to incorporate Cu into chitosan, including the addition of Cu nanoparticles (Tabesh et al., 2018) and doping with Cu (Alturki, 2022). Several studies have demonstrated the desired antibacterial activity of chitosan-copper complexes across various forms, including disks (Gritsch et al., 2018), coatings (Azizi Amirabad et al., 2023; Akhtar et al., 2020), and particles (Gholivand et al., 2023). Typically, these systems excel in enhancing the stability and bioavailability of the antibacterial agent, providing a controlled release mechanism, mitigating potential toxicity concerns, and minimizing treatment duration (Dzhardimalieva et al., 2019).

The body's extracellular matrix (ECM) is fabricated of proteoglycans and fibrous proteins, with fibers ranging from 60 nm to 120 nm (Young et al., 2016). Electrospinning is a method to construct nanofibrous mats which can simulate natural ECM. The nanofibrous and porous structure of the constructs produced by this approach improves oxygen exchange with the surrounding environment, is well-suited for cell development, promotes the adherence of human fibroblasts, and retains their distinctive shape. Furthermore, the high surface area of the electrospun mats leads to the effective release of loaded agents (Khil et al., 2003; Barnes et al., 2007; Vijayan et al., 2021). The polycationic structure and strong intramolecular hydrogen bonds of chitosan make it challenging for electrospinning; however, this limitation can be overcome via blending it with other polymers, including polyvinyl alcohol (PVA), PCL, polyethylene glycol (PEO), polylactic acid (PLA), silk fibroin, gelatin, collagen, and polyethylene terephthalate (PET) (Garcia Garcia et al., 2021). Among them, PVA is notable because it can effectively mitigate repelling interactions among chitosan chains, moderating the viscosity of chitosan solutions, and enhance molecular entanglement (Olvera Bernal et al., 2023). PVA is a water-soluble semi-crystalline polymer with attractive chemical and biological features, making it suitable for different biomedical applications (Kim et al., 2023). In the context of would management, PVA dressings exhibit non-adherent characteristics, minimizing the risk of trauma during removal (Huang et al., 2016). Incorporating PVA into chitosan also increases the mechanical characteristics of the obtained dressing by creating intermolecular and intramolecular hydrogen bonds and covering dressing drawbacks (Koosha and Mirzadeh, 2015, Panda et al., 2023).

The literature includes reports on the use of chitosan-copper complexes for wound management and the electrospinning of these complexes. Gholivand et al. (2023) incorporated chitosan-copper complex particles into a sodium alginate solution, poured into a calcium chloride cross-linking solution, and freeze-dried to develop antibiotic-free antibacterial dressings. Despite achieving a suitable balance of biocompatibility and antibacterial activity, this structure inherently lacks the ability to mimic the natural ECM and provide an optimal oxygen exchange capacity, which are advantages typically achieved through electrospinning. Azizi Amirabad et al. (2023) deposited chitosan-copper complexes/PVA electrospun coatings on a magnesium alloy to enhance its corrosion, antibacterial, and biocompatibility properties targeted for orthopedic applications. However, these nanofibers were not fabricated in a free-standing format suitable for wound dressing applications, nor were they specifically characterized for such purposes. In contrast, the present study introduces a novel and targeted approach to wound care by developing free-standing chitosan-copper complexes/PVA electrospun nanofibrous mats, which, to the best of our knowledge, have not been previously reported for wound dressing applications. This innovative approach combines the critical advantages of electrospinning—such as ECM-mimicking properties and enhanced oxygen exchange capacity—with the known antibacterial efficacy of chitosan-copper complexes. Unlike previous works, our study specifically addresses the needs of wound management by hypothesizing that these mats will provide a superior balance of antibacterial activity, cytocompatibility, and cell migration compared to existing constructs made from various combinations of chitosan, copper, and PVA. This research fills a significant gap by offering a material that is both functionally and structurally optimized for wound care, thus representing a meaningful advancement in the field.

2. Materials and methods

2.1. Materials

Chitosan)$C_6H_{11}NO_4$, deacetylation degree: 84.2 %, molecular weight: 140,469.4 g mol^{-1}, Sigma Aldrich, Germany) and PVA (C_2H_4O, fully hydrolyzed, Merck, Germany) were used as based and blending polymers, respectively. Anhydrous copper (II) chloride ($CuCl_2$, > 98 %, Merck, Germany) was used as the precursor of copper ions. Also, glacial acetic acid ($C_2H_4O_2$, 100 %, Sigma-Aldrich, Germany) and sodium hydroxide (NaOH, >98 %, Merck, Germany) were employed as the solvent and precipitant, respectively.

2.2. Sample preparation

Fig. 1 schematically represents the step-by-step fabrication process of fibrous wound dressings. Typically, the process involves the precipitation synthesis of chitosan-copper complexes and electrospinning of fibrous mats.

2.2.1. Synthesis of chitosan-copper complexes

Chitosan-copper complexes were prepared by an in-situ precipitation method as reported previously (Gritsch et al., 2018). Briefly, 0.406 g of chitosan was dissolved in a 2 % (v/v) aqueous solution of acetic acid under magnetic stirring at room temperature for 5 h to make a 2 wt% chitosan solution. Afterward, different amounts of $CuCl_2$ (Table 1) were loaded to the chitosan solution under stirring for 2 h to obtain homogeneous solutions with several ratios of Cu to NH_2 (X), as calculated using Eq. (1) (Gritsch et al., 2018).

$$m_{CuCl_2} = X.M_{CuCl_2}.m_{Chitosan}/\overline{M}_{Chitosan} \quad (1)$$

where m_{CuCl_2} and $m_{Chitosan}$ are the weights of the $CuCl_2$ and chitosan powders, while M_{CuCl_2} is the molecular weight of $CuCl_2$. Herein, $\overline{M}_{Chitosan}$ is calculated using Eq. (2), with DDA serving as the degree of deacetylation of chitosan, while $M_{Glucosamine}$ and $M_{N-acetyl\ glucosamine}$ are the molecular weights of glucosamine and N-acetyl glucosamine groups of chitosan, respectively.

$$\overline{M}_{Chitosan} = DDA \cdot M_{Glucosamine} + (1 - DDA) \cdot M_{N-acetyl\ glucosamine} \quad (2)$$

The precipitation of chitosan-copper complexes was obtained by the dropwise addition of a 0.1 M sodium hydroxide solution. This process indeed raises the pH and induces the ionization of chitosan, allowing it to bind with copper ions and leading to the formation of insoluble complexes (Rhazi et al., 2002). Finally, the collected chitosan-copper complex precipitates were rinsed with distilled water and then

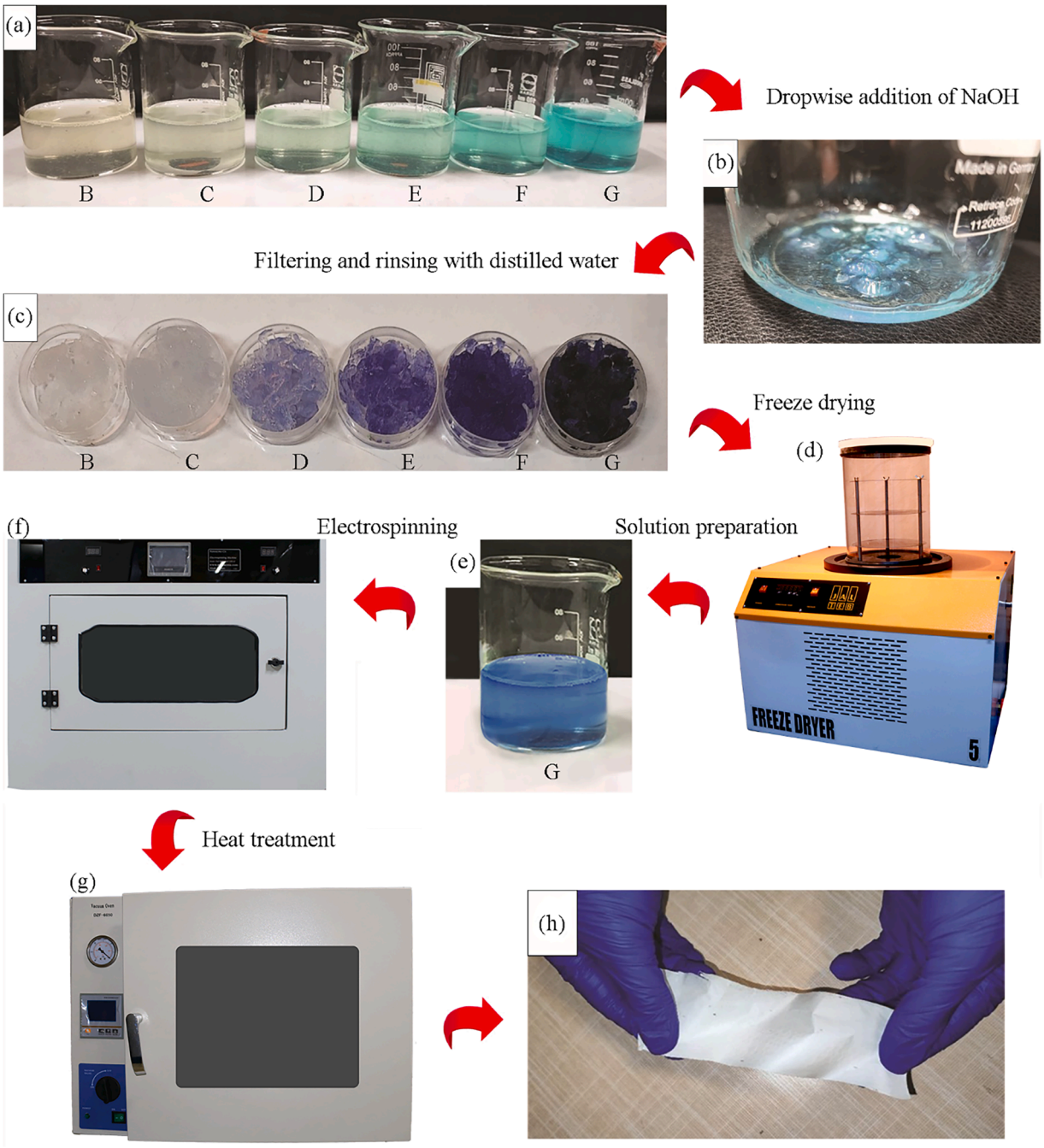

Fig. 1. Fabrication of chitosan-copper complexes/PVA electrospun mats: Chitosan solutions with the varying amounts of Cu (Table 1) (a), precipitation of chitosan-copper complexes by the dropwise addition of NaOH (b), collection of precipitants after rinsing with distilled water (c), obtaining chitosan-copper complex powders by freeze drying (d), preparation of electrospinning solutions by mixing chitosan-copper complexes solutions and PVA solutions in 30/70 ratio (e), electrospinning the mixed solution (f), crosslinking the detached mats by heat treatment (h), and final mats ready for further characterization (e).

Table 1
Specification of the samples prepared in this work.

Sample designation	$CuCl_2$ (mg)	Cu/NH_2 percentage
A	0.000	–
B	2.952	1
C	8.856	3
D	17.713	6
E	35.426	12
F	70.853	24
G	141.706	48

freeze-dried (Jal Teb) at -80 °C for 24 h.

2.2.2. *Fabrication of fibrous mats*

To optimize the concentration of electrospinning solutions, varying amounts of a prepared chitosan-copper complex (Sample C) were dissolved in a 2 % (v/v) aqueous solution of acetic acid at room temperature for 5 h to give concentrations of 2–3 wt%. PVA solutions with concentrations of 4–7 wt% were also made by dissolving PVA in distilled water at 90 °C for 3 h. The solutions were then mixed and stirred for 2 h at a volume ratio of 30:70 (chitosan or complex: PVA) to make homogeneous solutions (Table 2). These values were inspired from the literature (Koosha and Mirzadeh, 2015, Iqbal et al., 2020). After optimizing

Table 2
Specification of the samples prepared to optimize the concentration of electrospinning solutions.

Sample designation	Complex (wt %)	PVA (wt %)	Volume ratio (Complex: PVA)
C1	2	4	30:70
C2	2.5	5	30:70
C3	3	6	30:70
C4	3	7	30:70

the solution concentrations obtained at 3 wt% for chitosan/chitosan-copper complexes and 7 wt% for PVA, electrospinning solutions were prepared at the chitosan/chitosan-copper complex-to-PVA volume ratio of 3:7 using the same method.

A rotating cylindrical collector electrospinner (Nanoazma, Full Option Lab 2 ES I-II) was used to fabricate mats. The collector was covered with an aluminum foil. The prepared solutions were transferred to a 10 mL syringe with a 21-gauge needle and then placed in the syringe pump. The electrospinning distance was set at 14 cm, the applied voltage at 30 kV, the flow rate at 0.4, and the collector speed at 800 rpm. The electrospun mats were detached from the aluminum foil using sterile latex gloves and placed into a vacuum oven (TOB New Energy, DZF-6050) for heat treatment at 70 °C for 24 h.

2.3. Characterization

2.3.1. Viscosity and electrical conductivity of electrospinning solutions

The viscosity of the electrospinning solutions was explored by a Brookfield DV-111 ULTRA viscometer at a relative humidity of 26 % and 25 °C. Likewise, the electrical conductivity of the solutions was assessed by a portable conductivity meter (LH—C6).

2.3.2. Morphology of electrospun mats

The morphological features of the electrospun mats were examined using a field emission scanning electron microscope (FESEM, TESCAN, MIRA3, accelerating voltage: 15 kV). The ImageJ software was employed to analyze the size and size distribution of the fibers. Furthermore, the thickness of the mats was measured by a digimatic indicator (Mitutoyo Corp, ID-S112M, Japan). The pore size of a selected sample was also analyzed by the Barrett-Joyner-Halenda (BJH, BELSORP-mini II) method.

2.3.3. Molecular structure of electrospun mats

In order to ascertain the formation of the complexes and the mechanism by which chitosan uptakes copper, as well as to assess the influence of the varying copper quantities on the binding and crystallinity of the specimens, Fourier transform infrared (FTIR, AVATAR, Thermo, USA) spectroscopy was conducted on Samples A, B, C and G in the 4000–600 cm^{-1} range with a resolution of 4 cm^{-1} and an average scan number of 32.

2.3.4. Wettability of electrospun mats

Sessile water contact angle measurements were performed on Sample A as the control group, B with the lowest, and G with the highest copper amount to determine the effect of copper on hydrophilicity. For this purpose, a 5 μL droplet of distilled water with a surface tension of 72.8 mN/m and a density of 997 kg/m^3 was injected on the surfaces at a rate of 0.2 μL/s by a gauge with an external diameter of 700 μm. All were done at the temperature of 25 °C, the pressure of 88 kPa, and the relative humidity of 33 %. The angles were determined by the imageJ software.

2.3.5. Vapor permeability of electrospun mats

To assess the water vapor permeability, a 35-mL container was filled to 70 % of its capacity with deionized water. The electrospun mats of the same thickness (85 ± 1 μm) were cut and affixed to the aperture. The containers were then weighed prior to placing in a 37 °C incubator with a relative humidity of 30 % (W_i). The containers were weighed again after removing from the incubator after 24 h (W_f). The following formula was employed to determine the water vapor transmission rate (WVTR):

$$\mathrm{WVTR} = \left(\frac{W_i - W_f}{A}\right) \times 100 \quad (3)$$

where A is the area of the container opening.

2.3.6. Mechanical properties of electrospun mats

An SDL ATLAS machine was utilized to perform tensile testing to assess the tensile strength of the electrospun mats. The samples were cut into a 4 × 2 cm^2 rectangle with a thickness of 85 ± 1 μm. Measurements were conducted along the fiber alignment with the crosshead speed of 0.5 mm/min.

2.3.7. Degradation of electrospun mats

To evaluate the degradation rate of the samples, the mats were cut into 2 × 2 cm^2 dimensions. The initial weight of each sample (W_i) was measured using an HR-200 analytical balance. The specimens were subsequently submerged in phosphate-buffered saline (PBS) and transferred to an incubator set to 37 °C. At designated timeframes, the samples were removed and dried using a 40 °C oven. Following this, the ultimate weight of the dried samples was measured as W_f. The degradation rate was determined using the following formula:

$$\text{Degradation rate } (\%) = \left(\frac{W_i - W_f}{W_i}\right) \times 100 \quad (4)$$

2.3.8. Swelling of electrospun mats

In order to explore the swelling extent of the specimens, the mats were trimmed into 2 × 2 cm^2 dimensions. Subsequently, the samples were immersed in PBS and placed in a 37 °C Incubator. After specific time intervals, the specimens were taken out of the PBS solution, carefully blotted with a filter paper to remove any surface moisture, and then weighed again in their swollen states (W_s). The swelling degree was calculated using the below formula, with W_i representing the initial dry weight of each sample.:

$$\text{Swelling degree } (\%) = \left(\frac{W_s - W_i}{W_i}\right) \times 100 \quad (5)$$

2.3.9. Copper release from electrospun mats

To quantify copper release from the wound dressings, inductively coupled plasma optical emission spectroscopy (ICP-OES, SPECTRO Arcos) was utilized. 10 mg of the wound dressings with the low, moderate, and high copper amounts were immersed in 1 mL PBS for varying time intervals to evaluate the release behavior of the dressings. After each immersion period, the solutions were introduced to the ICP-OES set. By utilizing plasma, the specific wavelength associated with copper was detected, and the resulting data was reported in ppm.

2.3.10. Cytocompatibility of electrospun mats

The in vitro cytotoxicity of the mats was evaluated by the 3-(4,5-dimethylthiazol-2-yl)-2, 5-diphenyl tetrazolium bromide (MTT) assay with normal human dermal fibroblast (NHDF) cells. For this purpose, the cells underwent culturing in low-glucose Dulbecco's Modified Eagle Medium (DMEM) supplemented with 10 % fetal bovine serum and 1 % penicillin-streptomycin. Culture conditions were 5 % CO_2, 95 % humidity, and 37 °C. The specimens were punched and placed in 96-well plates. The mats were then sterilized by submersion in 70 % ethanol, followed by 15 min of UV irradiation. After that, 3 × 10^3 fibroblast cells were seeded on top of the mats in the 96-well plate, while the wells without the mats were considered as the control group (Zafari et al., 2020). The seeded cells underwent incubation at 37 °C and 5 % CO_2 for

24, 48, 72, and 120 h. After the period of incubation, 10 μl of the MTT solution at a concentration of 5 mg/mL was added into each well in order to induce formazan crystal formation. Subsequently, 100 μl of dimethyl sulfoxide (DMSO) was introduced into each well, followed by a 20-min agitation of the plates. The contents of the wells were relocated to fresh wells, and the absorbance of solubilized formazan was measured by an automatic microplate reader (BioTek, USA) set at 570 nm wavelength.

2.3.11. Cell migration of electrospun mats

The scratch assay was conducted to assess how the prepared samples influence the migration of NHDF cells. 2000 fibroblast cells were seeded onto 6-well plates and maintained at 5 % CO_2 and 37 °C until they reached 80–90 % confluency. Afterward, a sterile 100-μL pipette tip was employed to create a scratch on the cellular monolayer. Then, the wells underwent a gentle washing procedure using PBS in order to eliminate the scraped cells. The mats were cut into 1 × 1 cm^2 pieces, sterilized, immersed directly into the wells, and incubated at 37 °C with 5 % CO_2. After 24 h, the wound closure rate was monitored. Images were captured for each set using an inverted fluorescence microscope (Olympus, Japan). The ImageJ software was utilized to determine the surface area of the wound before and after incubation, and the results were expressed as a percentage of the initial scratch area at 0 h.

2.3.12. Antibacterial activity of electrospun mats

The antibacterial efficacy of the wound dressings against *Staphylococcus aureus* (*S. aureus*) and *Escherichia coli* (*E. coli*) bacteria was measured using the disk diffusion method. Bacterial suspensions with a density of 10^8 CFU/mL were first inoculated onto agar plates. These plates were then incubated for 24 h at a temperature of 37 °C. After immersing 10 mg of the wound dressings in PBS for 24 h, standard paper discs were smeared into 1 mL of this solution and carefully placed on the agar plates. The plates then underwent incubation at 37 °C for 24 h. Tetracycline was utilized as the positive control, while sterile discs smeared with PBS were used as the negative control. Finally, microbial inhibition zones around each disc were measured.

2.3.13. Statistical analysis

All of the tests were performed in triplicate, and the obtained data were statistically analyzed using SPSS software. Differences between the samples were evaluated using one-way analysis of variance (ANOVA), followed by the Tukey's post hoc test, at $p < 0.05$, $p < 0.01$, and $p < 0.001$.

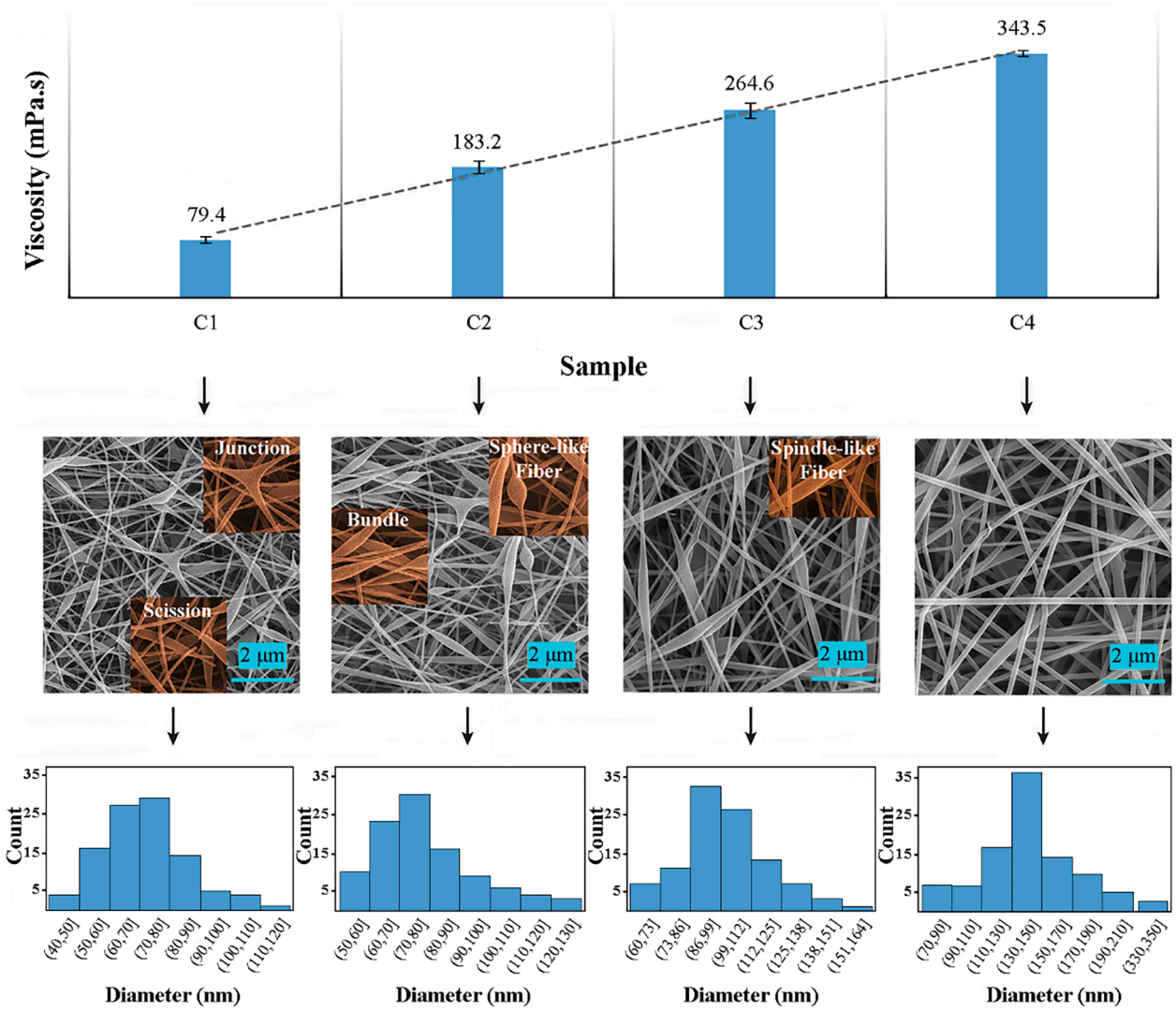

Fig. 2. Influence of the solution concentration and viscosity on the nanofiber morphology and diameter distribution.

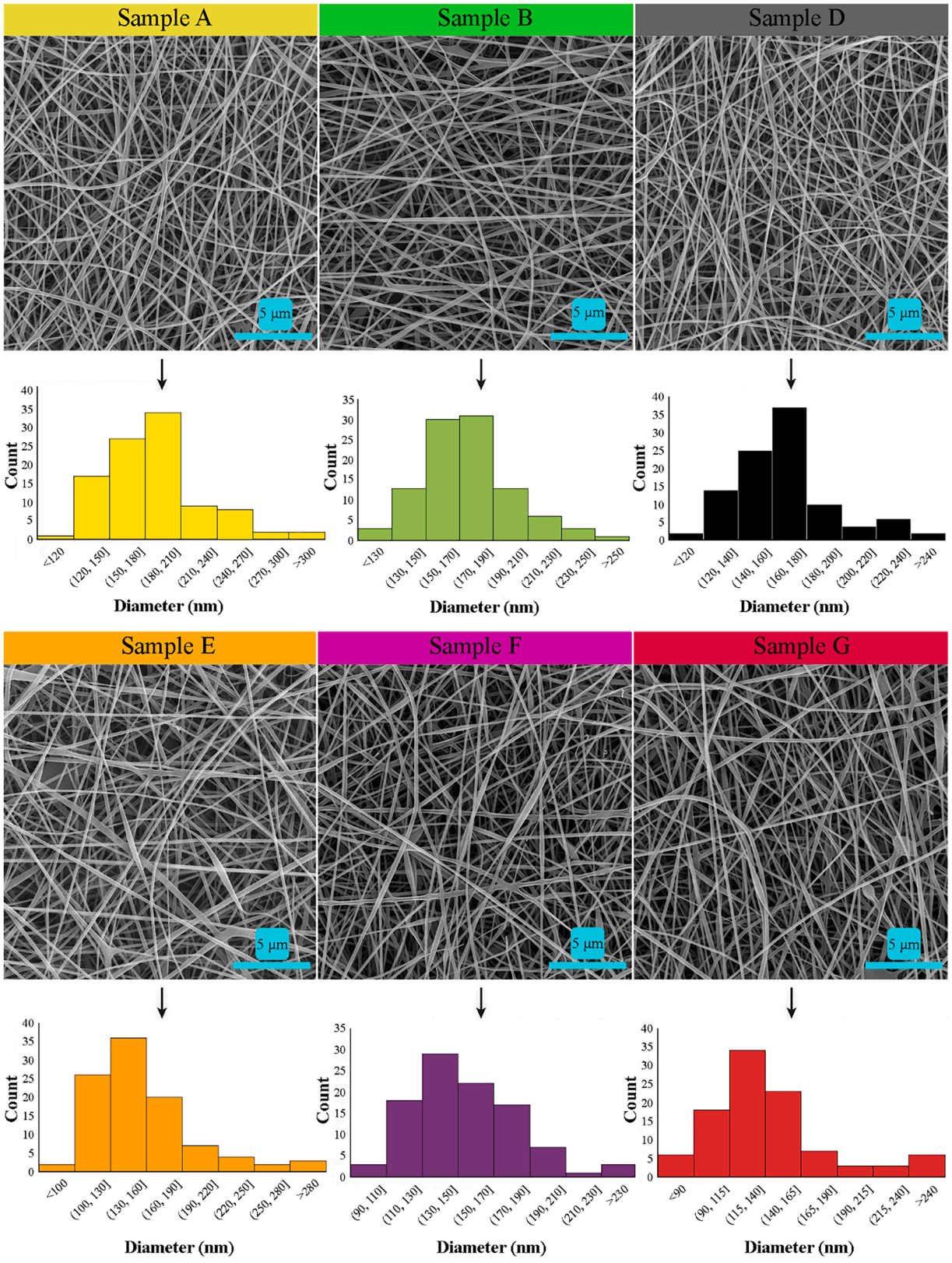

Fig. 3. Impact of the copper amount on the morphology and diameter distributions of the electrospun fibers.

3. Results and discussion

3.1. Electrospinning solution characteristics and morphology of wound dressings

The morphology of electrospun fibers is mainly controlled by the concentration of the electrospinning solution. To obtain nanofibers with desired morphology, solutions with various concentrations were scrutinized. The relation among the solution concentration, solution viscosity, and morphological characteristics of nanofibers is illustrated in Fig. 2. Spindles, junctions, bundles, and scission of nanofibers are four main defects that can be detected in the nanofibers formed from the low-viscosity solutions. By increasing the solution concentration, beads and spherical fibers were transformed into spindle-like fibers and eventually to uniform ones, which stems from the chain entanglement of the polymeric solution (Zhang et al., 2020).

The solutions of Samples C1 and C2 with the viscosities of 79.4 ± 4.4 and 183.2 ± 8.2 mPa.s, respectively, are dilute, in which chain interactions are minimal. It means that the concentration is below entanglement concentration, referring to the range of concentration in which entanglement occurs. Accordingly, the nanofibers are rife with the defects listed above. Indeed, some fibers reach the collector while not entirely being dried under the used voltage during the tip-to-collector destination, leading to the formation of junctions and bundles. Additionally, scissions in the fibers are attributed to the solution's inadequate surface tension (Abutaleb et al., 2017). Sample C3, whose solution possesses a viscosity of 264.6 ± 10.1 mPa.s, is classified as semi-dilute, in which polymer chains start to interact with each other and affect viscosity. However, there is no evidence of significant polymer chain entanglement; hence, the structure retains spindle-like fibers (Rahmati et al., 2021). Sample C4 with a solution viscosity of 343.5 ± 9.1 mPa.s is a concentrated solution, so that polymer chains are entangled and the solution exhibits a viscoelastic behavior. The nanofibers fabricated from this solution are defect-less and have been identified as the samples with a promising viscosity.

The diameter distribution of the nanofibers is also indicated in Fig. 2. There is a direct correlation between the diameter of the nanofibers and the viscosity of the solution. The nanofibers formed from a solution exhibiting a viscosity of 79.4 ± 4.4 mPa.s possess an average diameter ranging from 60 to 70 nm. On the other hand, the nanofibers obtained from the solution with a higher viscosity of 343.5 ± 9.1 mPa.s have a more extensive range of diameters from 130 nm to 150 nm. This can be attributed to the decreased speed of the polymeric solution in the samples with lower copper contents having higher surface tension and lower electrical conductivity during the needle-collector deposition process.

Once the optimal concentration for electrospinning the chitosan-copper complex/PVA solution was determined, Samples A through G were subjected to electrospinning using a blend containing 3% wt chitosan-copper complexes and 7% wt PVA. The morphology of the fibers generated from the electrospinning of these solutions, accompanied by their respective diameter distributions, is depicted in Fig. 3 (except for Sample C which was illustrated as C4 in Fig. 2). Sample A, consisting solely of chitosan and PVA, presents a viscosity of 870.0 ± 7.1 mPa.s, which is approximately two times greater than that of Sample B, the sample with the lowest copper amount. Consequently, this sample provides the greatest fiber diameter when compared to the other ones. The fiber diameter distribution observed for the given sample is between 180 nm to 210 nm.

The presence of a higher quantity of copper within the chitosan-copper complex results in a significant drop in the viscosity of the polymer solution. Specifically, the solutions of Samples B, C, and G exhibit a reduction in viscosity to 389.0 ± 3.5, 343.5 ± 6.7, and 296.1 ± 7.3 mPa.s, respectively. As a consequence of this reduction in viscosity, the fiber diameter is likewise reduced. The most probable rationale for this phenomenon can be the diminished quantity of hydroxyl (OH) groups in the complex in comparison to pure chitosan. By introducing the powder, which contains hydroxyl groups, into the solvent, hydrogen bonding occurs, resulting in the formation of interconnected chains and bigger molecules with intermolecular interactions. Sample A, which has the highest concentration of hydroxyl groups, has a larger molecular size, which displays higher resistance to molecule movement and, as a consequence, a greater viscosity. Similar outcomes were obtained when Lončarević et al. (Lončarević et al., 2021) synthesized chitosan-copper microspheres. In comparison to pure chitosan, solutions containing the minimum amount of copper exhibited a 1.35-fold decrease in viscosity, whereas the solution containing the maximum quantity of copper demonstrated a 2.4-fold decrease. This reduction was attributed to alterations in the configuration of polymer chains and the occupation of amino and hydroxyl groups by the introduction of Cu^{2+} (Costa et al., 2015). It is postulated that these groups have ceased to participate in hydrogen bonding, either intrachain or interchain. The observed substantial reduction in viscosity by them implies that a greater quantity of ligands, originating from either the same or distinct chains, is engaged in coordination with the copper (II) ions.

Another factor contributing to the reduction of the fiber diameter is the increase in electrical conductivity as a result of the copper addition. The electrical conductivity of Sample A, which includes no copper, is 1426 ± 10 μS/cm, while Sample B with one percent copper has an electrical conductivity of 2130 ± 13 μS/cm. The increased electrical conductivity of the solution leads to a more pronounced impact of the applied voltage of electrospinning, causing the solution to move faster toward the collector and consequently reducing the fiber diameter.

The oxygen permeability of wound dressings is vital for wound healing. The porosity of a wound dressing determines its gas permeability. The nano-sized pores of the constructs produced by the electrospinning process is its most advantageous feature, which distinguishes it from other synthesis methods. The BJH analysis of a selected sample, Sample E, demonstrated that the final mat with the thickness of 85 ± 1 μm possesses an average pore size of 16.0 ± 0.3 nm, categorizing it as a mesoporous material. Not only this pore size corresponds to the kinetic diameter of O_2 molecules (3.46 Å) (Kentish et al., 2008), but also it can prevent bacteria from penetrating to the wound bed. This is because *S. aureus* with a spherical morphology has a diameter ranging from around 0.5 μm to 1 μm, and *E. coli* with a rod-shaped morphology is almost 2 μm in length and 0.5 μm in diameter (Feng et al., 2022, Turishchev et al., 2020).

3.2. Molecular structure of wound dressings

The FTIR spectra of the specimens are shown in Fig. 4a. N—H and O—H stretch vibrational frequencies of chitosan, as well as intermolecular and intramolecular bindings of PVA, are all associated with broad absorbance peaks between 3150 and 3500 cm^{-1} wavenumbers (Paluszkiewicz et al., 2011). Losing the sharpness of this peak, absorbing less infrared light, and shifting to lower wavenumbers by increasing the copper amount are three evidences that point to the participation of amine and hydroxyl groups in chitosan-copper complex formation, with the absence of free O—H and N—H groups in the samples with the high copper amounts. This is in contrast to the doping method in which chemical bonds are fewer and the shift of chitosan amine and hydroxyl peaks is minimal (Sportelli et al., 2016). Two peaks at 2800 and 2900 cm^{-1} are assigned to the symmetric and asymmetric vibrational modes of the CH_2 group, respectively (Mekahlia and Bouzid, 2009). The small peak at 1650 cm^{-1} also shows the C = O stretch of the amide band that is rarely present in the structure because of the non-deacetylated groups of chitosan. The presence of a strong peak at 1250 cm^{-1} indicates the formation of a chemical link between the C–O of the CH_2OH group in chitosan and the OH group in PVA (Abbas et al., 2020). Two peaks in 1025 and 1079 cm^{-1} are attributed to the stretching of the glycosidic bond C—O that connects the glucosamine monomers of chitosan. The 1025 cm^{-1} peak is stretching of carbon number 6 in chitosan (primary OH^-), and 1079 cm^{-1} is stretching of carbon number 3 (secondary OH^-)

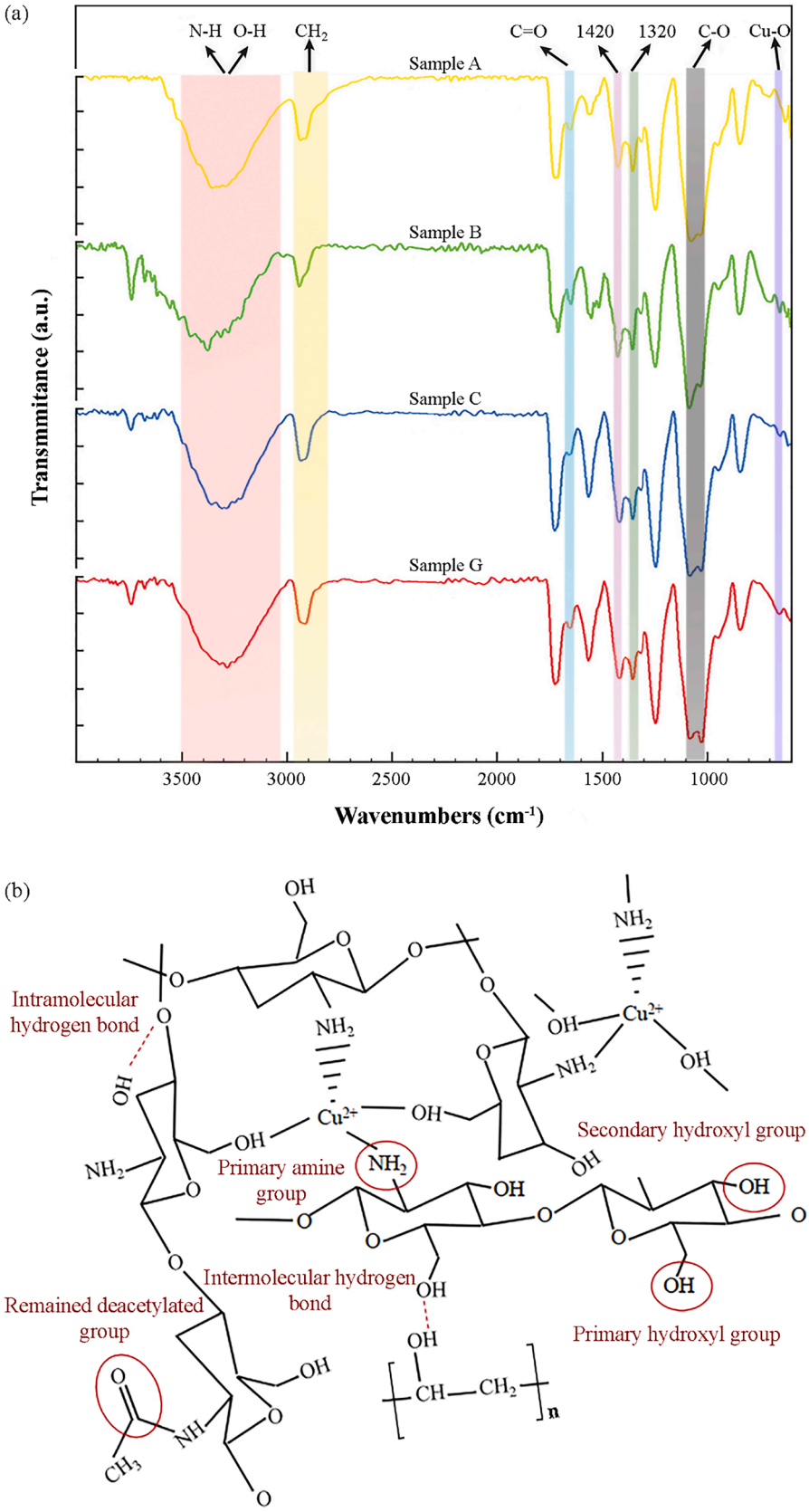

Fig. 4. FTIR spectra of the selected samples (a) and FTIR-derived structure of the chitosan-copper complex/PVA nanofibrous mats (b).

(Nikonenko et al., 2005). Increasing the copper amount leads to a reduction in the intensity of the primary hydroxyl groups relative to the secondary hydroxyl groups, indicating a greater involvement of primary OH groups in the formation of the complexes. This fact alongside with the appearance of a new peak at around 650 cm^{-1}, which is associated with M-O bonding, confirms the incorporation of copper in terms of complex into the structure of chitosan (Rashid et al., 2021).

Chitosan is a polymer with a semicrystalline structure, and its degree of crystallinity is subject to several factors. One of the factors under consideration is the degree of deacetylation, which exhibits a direct correlation with the ratio of the absorption peak at 1420 cm^{-1} to 1320 cm^{-1} (Rohyami and Sari, 2021, Sánchez-Machado et al., 2024). Notwithstanding using identical chitosan and applying a similar processing procedure, this ratio is much greater for Samples B and C in comparison to pure chitosan/PVA and the complexes with the elevated copper concentrations. Consequently, it can be inferred that the presence of copper in very low concentrations promotes the formation of crystalline structures. In contrast, the higher concentrations seem to interfere with the regularity of the structural arrangement.

The uptake of copper by chitosan occurs through either bridge or pendant models (Pestov and Bratskaya, 2016), which is confirmed by the FTIR analysis, where the hydroxyl and amine groups of chitosan take part in the complex formation. It is observed that the samples containing the lower amounts of copper exhibit higher crystallinity and a tightly packed structure. This suggests that the bridge model is dominated when copper is introduced in low amounts, in which copper ions form coordination bonds with two or more chitosan chains, bridging them together and forming a three-dimensional packed network (Fig. 4b). On the other hand, the lower crystallinity of the samples with the high copper amounts goes well with the characteristics of the pendant model, in which the structure is not packed. These findings also support the viscosity results of the electrospinning solutions, where viscosity decreased with the addition of the high copper amounts.

3.3. Wettability of wound dressings

Fig. 5a displays the contact angle results for Samples A, B, and G, demonstrating the impact of copper complexation on the hydrophilicity of the wound dressings. Sample A exhibits a contact angle of 89.5° ± 2.4°, while Sample B shows an increased contact angle of 125.5° ± 3.9° This increase is attributed to the influence of copper complexation on chitosan crystallinity and the occupation of hydrophilic functional groups, such as hydroxyl and amino groups, as confirmed by FTIR analysis. This trend is supported by studies that demonstrate a direct correlation between the fiber diameter and hydrophilicity of electrospun mats (Cui et al., 2008). Nevertheless, Sample G, which contains the highest copper concentration, demonstrates a decreased contact angle of 93.5° ± 5.2°, indicating a resurgence in hydrophilicity in comparison to Sample B. This change is likely due to alterations in surface roughness (Fig. 5a) and fiber crystallinity. Typically, Sencadas et al., (2017) reported a direct relationship between water contact angle and fiber crystallinity in electrospun fibers. This supports the observed decrease in

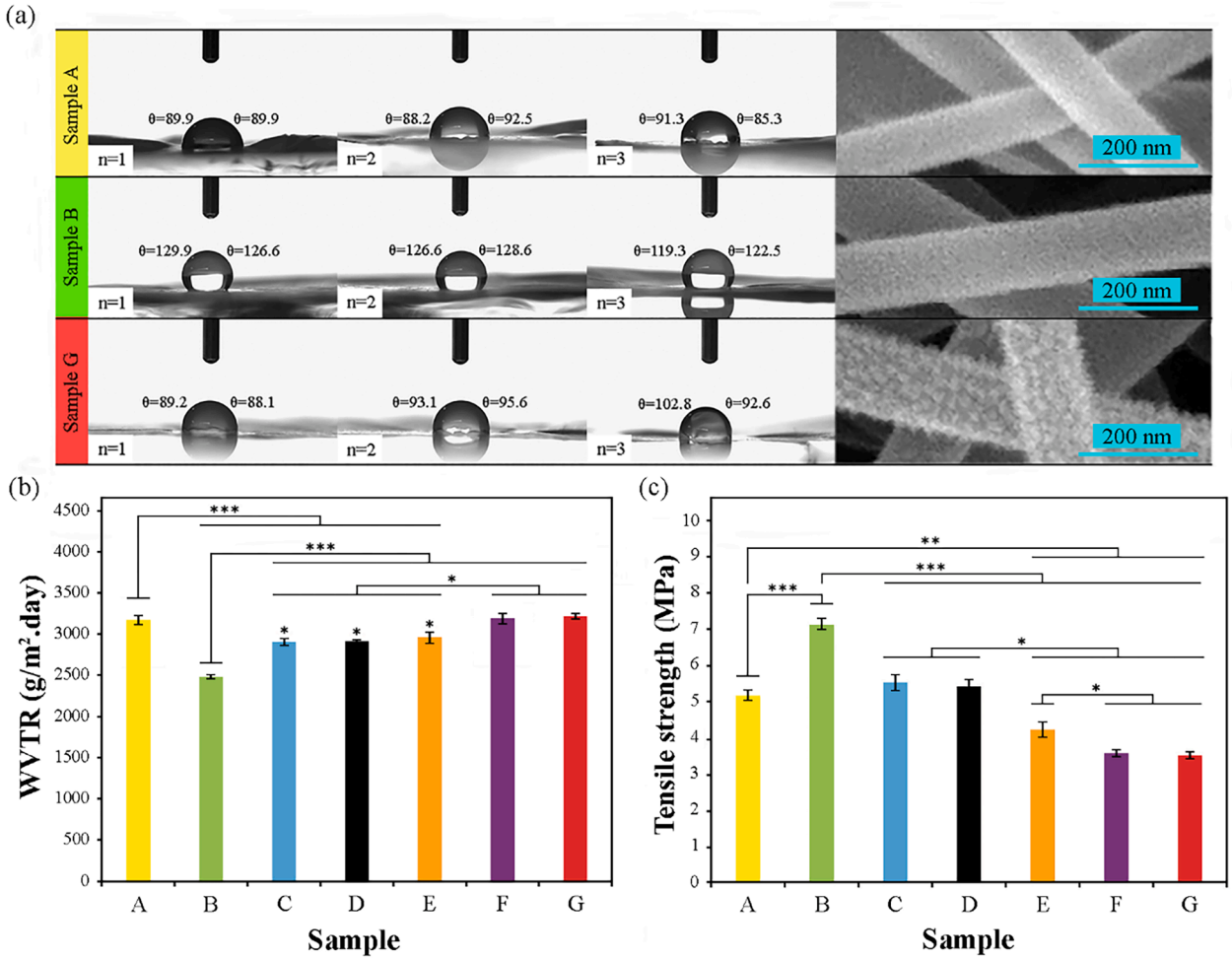

Fig. 5. Images of water droplets on selected mats, involving chitosan/PVA and chitosan complexed with the low and high copper amounts/PVA (a), WVTR of the electrospun mats (b), and effect of the amount of copper on the tensile strength of the wound dressings (c), with *, **, and *** denoting statistically significant differences with $p < 0.05$, $p < 0.01$, and $p < 0.001$, respectively.

the contact angle of Sample G, which has the lowest crystallinity based on the FTIR analysis.

3.4. Water vapor transmission of wound dressings

Fig. 5b displays the experimental WVTR of the mats. Sample B has an exceptionally lower WVTR compared to the other samples. Two primary factors contribute to the reduced WVTR. First, this mat exhibits a less degree of wettability, which negatively impacts its WVTR. Second, the sample displays the bridge binding model with higher levels of crystallinity, resulting in an ordered and densely packed structure that impedes the passage of vapor and consequently leads to a lower WVTR. The WVTR of the other samples exhibits no significant differences. It seems that the positive impact of the wettability of Sample A is somewhat counterbalanced by the decrease in the fiber size and porous structure of Samples C, D and E. The improved porous structure of the mats plays a favorable function in WVTR by creating more spaces to permit vapor transition. Samples F and G show a bit higher WVTR in comparison with Sample A. The reason is that they possess finer fibers with almost equivalent hydrophilicity as Sample A.

3.5. Mechanical properties of wound dressings

Chitosan possesses a rigid structure primarily attributed to the

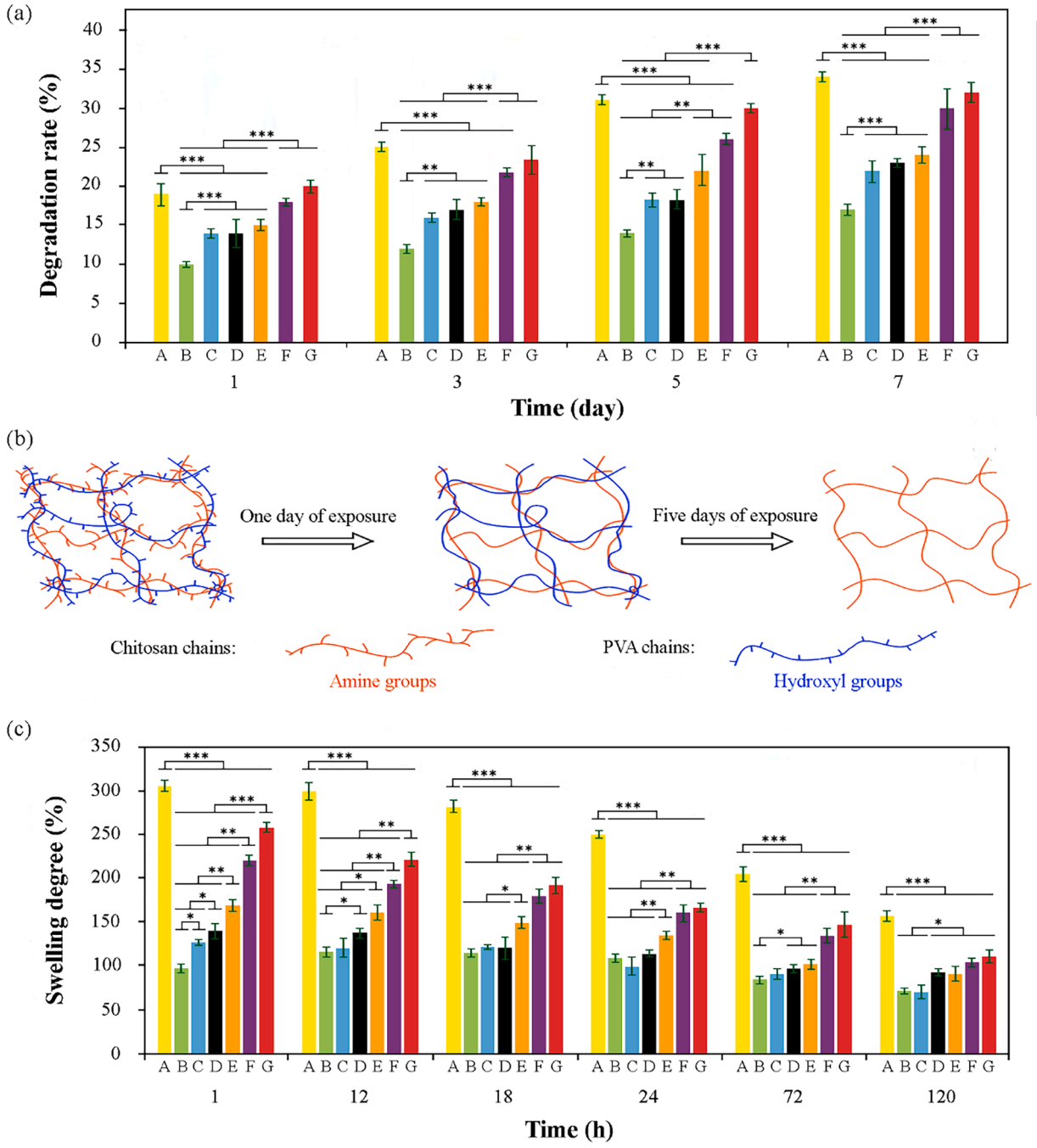

Fig. 6. Relationship between the copper concentration and degradation rate in the electrospun nanofibrous mats (a), schematic illustration of the multi-step degradation process of the wound dressing nanofibers (b), and relationship between the copper concentration and swelling degree in the electrospun nanofibrous mats (c), with *, **, and *** denoting statistically significant differences with $p < 0.05$, $p < 0.01$, and $p < 0.001$, respectively.

presence of acetyl groups, intermolecular hydrogen bonding, and the d-glucosamine component. Although this inherent rigidity can lead to the brittleness of materials made from it, blending chitosan with PVA has emerged as a promising approach to enhance flexibility and mechanical properties, effectively mitigating the brittleness issue of chitosan-based materials (Koosha and Mirzadeh, 2015, Abraham et al., 2016).

The tensile strength of the samples is provided in Fig. 5c. Sample A exhibits a tensile strength of 5.15 ± 0.16 MPa, whereas Sample B demonstrates a higher tensile strength of 7.11 ± 0.17 MPa. The observed increase can be elucidated by considering two primary factors. First, the higher tensile strength exhibited by Sample B can be attributed to its enhanced crystallinity, indicative of stronger bonding within the material. The heightened crystalline structure contributes significantly to the overall mechanical strength of the sample. Second, a reduction in the nanofiber size constitutes another influential factor. This decrease in the fiber dimensions in Sample B results in improved strength compared to Sample A. The diminution in the nanofiber size is believed to enhance interfacial interactions and bolster the structural integrity of the material, thereby leading to the observed augmentation in tensile strength. Consistent with the results of the current study, Rácová et al. (Rácová et al., 2014) demonstrated that incorporating cupper ions into PVA fibers can improve their tensile strength and elongation. This further corroborates the outcomes of the present paper. On the contrary, the addition of higher copper contents demonstrates a reduction in the tensile strength of the nanofibers, where Sample G, characterized by the highest copper content meets 3.41 ± 0.11 MPa. The diminution in tensile strength can be traced to both the low levels of crystallinity detected in this sample and the more random alignment of the fibers in comparison to the other samples, as shown in Fig. 3. The optimal range of tensile strength for wound dressings is 1–32 MPa, dependent on various factors including the properties of human skin and the type of wound being treated. Typically, the dressings developed in the current work is well-suited to treat relatively shallow wounds within a short time period from the mechanical perspective (Farshi et al., 2022).

3.6. Degradation of wound dressings

Fig. 6a shows the degradation rate of the different samples after heat treatment at 70 °C. The contribution of PVA to degradation, which is influenced by the replacement of its internal hydrogen bonds with hydrogen bonds between the polymer and water molecules (Jayasekara et al., 2005) is similar for the different samples as they have a similar amount of PVA. The degradation process of chitosan involves the hydrolytic cleavage of glycosidic bonds within the polymer's structure. Sample A contains a higher concentration of free amine and hydroxyl groups, giving rise to accelerated degradation relative to the other samples. This sample has lost 19 ± 2 % of its initial weight on the first day and 34 ± 1 % in seven days. The other samples are less degraded than Sample A due to the presence of fewer free amine and hydroxyl groups. Sample B exhibits the least amount of degradation across all time intervals. This can be attributed to its high crystallinity and hydrophobicity. The degradation rate exhibits a direct relation with the copper concentration among the remaining samples. This can be related to the presence of weak electrostatic bonds within the structure of the samples with the high copper amounts.

The degradation rate of the samples becomes relatively stable after the initial day. Nevertheless, the results suggest that there is a resurgence in the degradation rate of Samples F and G, highlighted by a high copper content, throughout the period spanning from 3rd day to 5th day. Likewise, it is seen that Samples C, B, and D, which possess relatively lower copper concentrations, exhibit an escalation in the degradation rate during the period ranging from 5th day to 7th day. The observed phenomenon can be attributed to the breakdown of PVA within the structure, which initiates at a later stage in the samples with the lower copper concentrations with denser crystal structures. Based on the information provided, it is believed that the degradation of the chitosan-copper complex/PVA wound dressings takes place in three distinct steps, as schematically depicted in Fig. 6b. The first step involves the degradation of linking chains of the polymers, where copper is present and bonded, which may occur relatively quickly. The second step is related to the degradation of PVA chains, which may begin after three or five days of exposure. Step 3 involves the breakdown of primary chitosan chains, which would not commence within seven days.

3.7. PBS uptake capabilities of wound dressings

The results of the swelling behavior of the samples which show their exudate uptake capabilities are depicted in Fig. 6c. Upon immersion in PBS, Sample B exhibits a comparatively lower absorption capacity than Sample A. Sample B absorbs a mere one-third of the liquid and experiences a swelling degree of 98 ± 4 % within the initial hour, while Sample A absorbs 305 ± 6 % at the same time. It appears that the addition of copper within the complex is negatively correlated with the swelling degree. The results obtained from the FTIR analysis indicated that the chitosan-copper complexes exhibit a diminished number of unbound primary hydroxyl groups in comparison with the control sample that has no copper. One hydrogen atom is covalently bonded to one oxygen atom to form the hydroxyl group, leading to a tendency to absorb water molecules as a result of the significant electronegativity of oxygen.

Based on Fig. 6c, by increasing the copper content, the degree of swelling recorded in the samples exceeds that of Sample B. Sample C demonstrates a degree of swelling of 125 ± 3 %, and this trend continues as the Sample G's degree of swelling increases to 258 ± 6 % within the initial hour. The decreased crystallinity observed in the samples can account for this behavior. It has been determined by the FTIR analysis that the increased concentrations of copper disrupt the compact structure of the samples. As a result, a higher quantity of polymer chains is rendered permeable to water molecules. Furthermore, copper ions at higher concentrations are released at earlier stages. As a result, the primary amine and hydroxyl sites, which were previously occupied by copper, become available for water-molecule interactions. With the exception of Sample B, which experiences additional swelling and reaches a degree of 116 ± 6 %, the majority of the samples reach a swelling equilibrium within the initial 12-hour period. The degree of swelling in all the samples subsequently begins to decrease. The greater reductions in the swelling degree measured in Samples A and G after 5 days, as opposed to the initial hour results, can be attributed to the degradation of the samples, where they lost around 34 % of their initial weights.

Overall, the findings indicated that the developed dressings with at least 12 % copper exhibits a high swelling capacity (> 150 %) within the first 24 h, classifying them as highly absorbent constructs. On the one hand, this property promises that the dressing will effectively manage wound exudates, promoting a moist wound environment that facilitates cell recruitment and migration. On the other hand, the high swelling capacity of the dressing makes it a suitable candidate for applications requiring a controlled release of therapeutic agents (Feng and Wang, 2023).

3.8. Copper release kinetics from wound dressings

In order to analyze the rate at which copper is released from the nanofibers, ICP analyses was performed. The results of this study, which is illustrated in Fig. 7a and b, suggest that all the three samples exhibited a burst release of copper ions. The occurrence of this phenomenon can be ascribed to the particular configuration of the chitosan-copper complexes. As previously stated in the degradation section, the first step in the degradation of the chitosan-copper complex is the breaking of weak intermolecular bonds between polymers linking chains. Given the preponderance of copper ions that are situated within these particular regions, the accelerated swelling of the samples additionally supports the rapid release of copper ions at initial stages (Safdar et al., 2019).

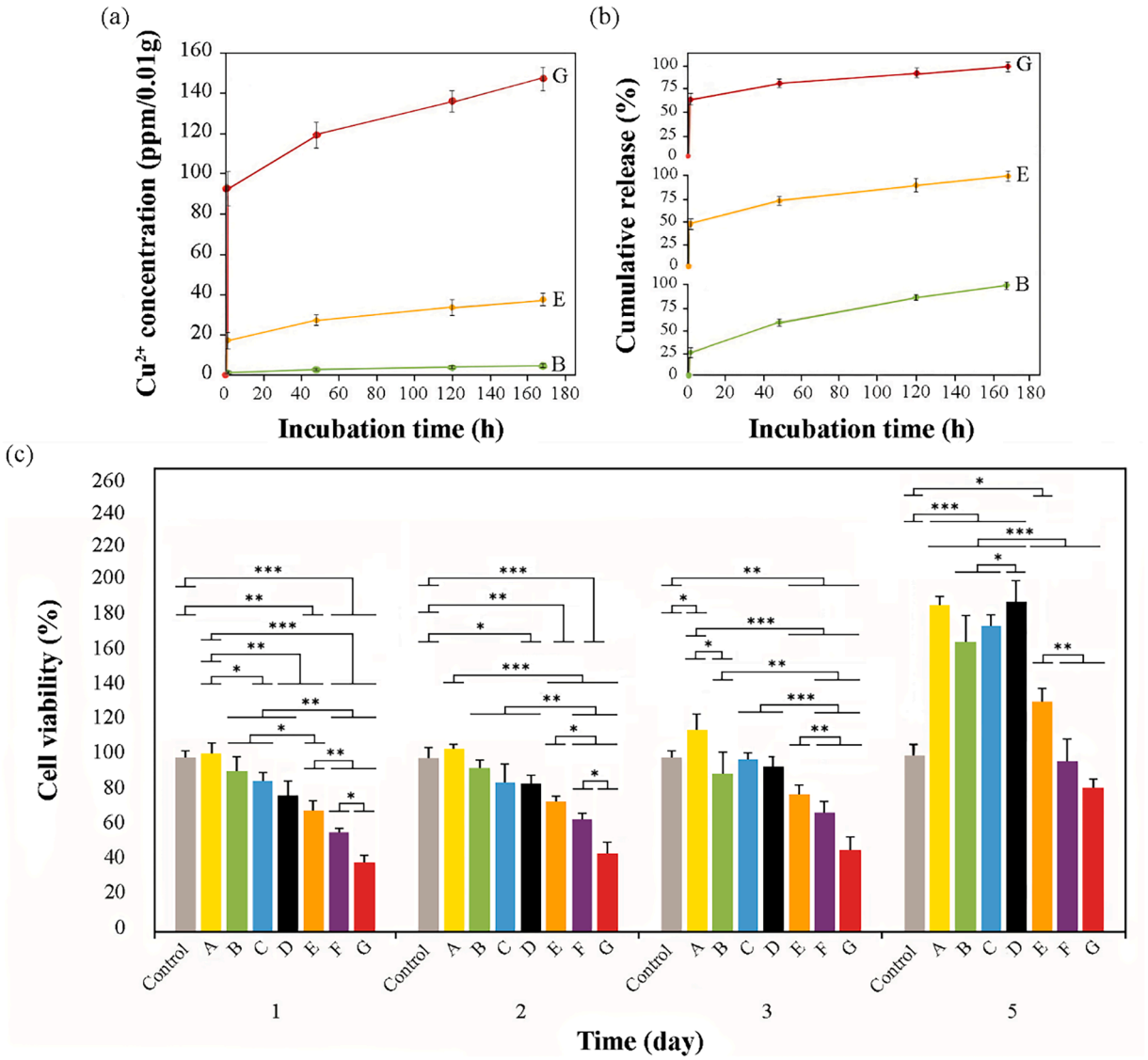

Fig. 7. ICP-OES detection of copper release from the electrospun nanofibrous mats at time points over 7 days (a). Cumulative copper release profile from the nanofiber mats as a function of immersion time in PBS (b). In vitro cell metabolic activity on the samples containing the varying contents of copper (c), with *, **, and *** denoting statistically significant differences with $p < 0.05$, $p < 0.01$, and $p < 0.001$, respectively.

In the first hour, Sample G, with 48 % copper, demonstrated a 63 ± 5 % release, corresponding to 92.1 ± 8.1 ppm of its total copper release across a seven-day duration which amounted to 146.9 ± 5.6 ppm. Sample E, which possesses a copper level of 24 %, exhibited a release of 46 ± 5 % within the initial hour. This release corresponds to a value of 17.2 ± 3.8 ppm in terms of the total copper release over a period of seven days, which amounts to 37.3 ± 2.9 ppm. Similarly, Sample B, with 1 % copper, showed a 25 ± 4 % copper release in the first hour, equivalent to 1.0 ± 0.6 ppm of its total 4.1 ± 0.8 ppm copper release. By increasing the loaded copper content, both the concentration of released copper and the cumulative release percentage are elevated. It is attributed to the higher copper concentration gradient, greater swelling capacity (Fig. 6c), and increased structural irregularity with weaker electrostatic bindings (Fig. 4) associated with the higher loaded copper content. Additionally, applying a voltage of 30 kV during the electrospinning process likely causes weakly bonded copper ions to migrate toward the surface of the nanofibers, further enhancing their release.

Following the initial rapid burst release, the subsequent release rate of copper from the nanofibrous wound dressings exhibited a sustained and prolonged pattern, due to the chemical bindings which were demonstrated by FTIR. This observed release profile exhibits significant benefits in terms of the wound dressing efficacy. The initial rapid release of copper promotes the elimination of any pre-existing bacteria within the wound bed. The gradual and sustained release of copper ensures the maintenance of antimicrobial levels within the wound area, thereby effectively inhibiting subsequent bacterial invasion and any possible infection (Guo et al., 2022). Furthermore, the continuous presence of copper has the potential to induce cell proliferation and enhance the overall process of wound healing (Xiao et al., 2017).

3.9. Cytocompatibility and cell proliferation

Cell metabolic activity was assessed by the MTT assay, and the results are presented in Fig. 7c. Sample A, which contains only chitosan and PVA, exhibited a small augmentation in cellular metabolic activity following a single day as it has been demonstrated that chitosan can modulate cell behaviors, such as proliferation, and migration (Caetano et al., 2015). The samples containing up to 6 % copper demonstrated favorable biocompatibility and did not exhibit any toxic effects on fibroblast cells after the first day of exposure. Sample D had an acceptable level of cell metabolic activity at 78.4 ± 7.9 %, and Sample E with 12 % copper showed a mediocre cell metabolic activity of 69.5 ± 5.3 %.

Conversely, Samples F and G, with the copper ion levels of 24 and 48 % resulted in notable cytotoxicity, as evidenced by cell metabolic activity of 57.0 ± 1.9 and 35.1 ± 3.3 %, respectively. The high toxicity of the first day's results is in correspondence with the ICP results of copper release, which showed a burst copper release. Copper ion toxicity primarily arises from its binding to sulfhydryl (-SH) and thiol groups in proteins (Letelier et al., 2005), disrupting biological functions and leading to iron deficiency (Letelier et al., 2010). Additionally, copper interferes with cellular signaling pathways regulated by Cu-dependent proteins and promotes the generation of reactive oxygen species (ROS) through redox and Fenton reactions (Chen et al., 2019, Kardos et al., 2018). This ROS production causes oxidative stress, damaging cellular components, disrupting energy production, signaling pathways, and gene expression, ultimately leading to cellular dysfunction and death (Dash et al., 2023).

During the second day, there was a modest reduction in toxicity in all of the samples, as evidenced by the increase in cell metabolic activity observed in Samples D and E. Notably, these samples exhibited the most substantial improvement, with cell metabolic activity being around 6 % higher than the results obtained on the first day. These results demonstrate that fibroblast cells activate their antioxidant defense mechanism in response to oxidative stress and adapt to copper ions (Gaetke and Chow, 2003). Metal-binding proteins primarily achieve this adaptation by regulating the toxicity of copper ions, providing an additional advantage of metallic ions over antibiotic drugs, which have more intricate cellular adaptation mechanisms (Godoy-Gallardo et al., 2021). During the third day of the experiment, there was a further increase in the cell proliferation and metabolic activity. Sample A exhibited a cell metabolic activity of 115.9 ± 8.7 %, indicating a healthy cell population. In contrast, Samples F and G maintained their toxic effects, as evidenced by cell metabolic activity of 62.5 ± 5.5 and 39.2 ± 6.1 %, respectively. On the fifth day, it was observed that all the samples exhibited a notable augmentation in metabolic activity. Sample G, which exhibited significant toxicity on the first, second, and third days, demonstrated a cell metabolic activity of 72.5 ± 3.9 %, while Samples D and A exhibited the highest levels of performance, as evidenced by cell metabolic activity of 189.1 ± 11.6 and 186.9 ± 4.5 %, respectively.

Khan *et al.* (Khan et al., 2024) reported a Vero epithelial cell viability of 70 % for antibacterial PVA/chitosan/copper oxide electrospun dressings, whereas a higher fibroblast cell viability of 78.4 ± 7.9 % with the same antibacterial performance was achieved in the present study within the same time frame. Although direct comparison is challenging due to the use of different cell types, the observed disparities in the copper release profile provide insight into these cytotoxicity results. Typically, a substantial burst release of copper oxide nanoparticles was observed within the initial 6 h in that study, which is likely responsible for the higher initial toxicity. In contrast, the current work demonstrates a more sustained release of copper over one week owing to coordinate chemical binding in complexation, leading to a more controlled release and higher cytocompatibility.

3.10. Cell migration of wound dressings

The results of the cell migration (Fig. 8a) and the percentage of wound surface closure (Fig. 8b) demonstrate a direct correlation between the copper ion concentration and cell migration up to a certain limit. The fabricated nanofibrous mat with 6 % copper yielded the most favorable results, enhancing cell migration significantly when compared with Sample A. Samples C and B with 3 and 1 % copper, respectively, also promoted cell migration, although the effect was less pronounced than that of the 6 % copper variant. Copper ions are essential trace elements involved in various biological processes. These ions have been indicated to stimulate the creation and deposition of ECM components, like collagen and elastin, which are critical for cell adhesion and migration (Maquart and Monboisse, 2014). However, there is a decrease in the cell migration with an increase in the copper concentration

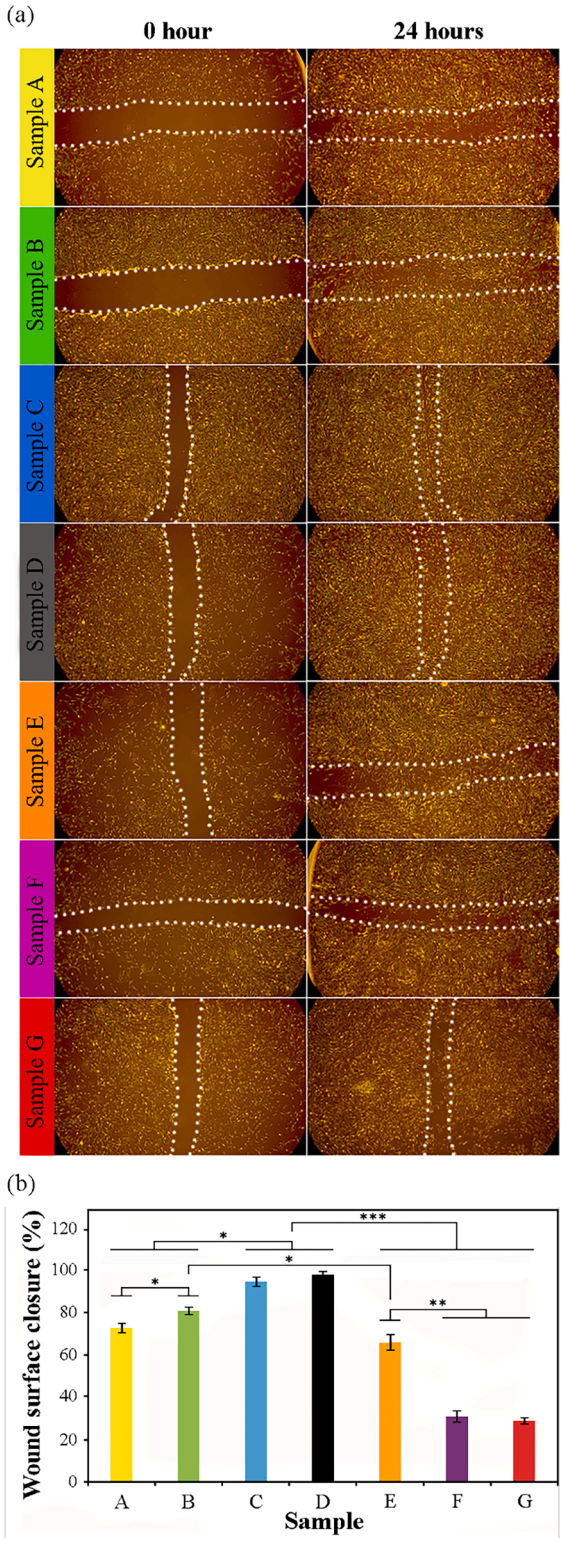

Fig. 8. Representative photomicrographs obtained from in vitro scratch wound healing assays (a). Impact of the different samples on the percentage of wound surface closure, measured using ImageJ (b), with *, **, and *** denoting statistically significant differences with $p < 0.05$, $p < 0.01$, and $p < 0.001$, respectively.

beyond the optimal value of 6 %, where there is no statistically significant difference between the samples with 12 % copper and the control. The nanofibers with 24 and 48 % copper ions exhibited poor cell migration, even much lower than that of the chitosan-PVA control. This pattern suggests that while a certain level of copper ions is beneficial for cell migration, excess copper concentrations may have a detrimental impact. A plausible explanation for this pattern could be related to copper toxicity, as discussed above.

Sandra *et al.* (Sandra et al., 2024) reported that electrospun dressings made from PVA/chitosan incorporating CuO nanoparticles offered a wound closure rate of 85 % within 24 h in a NIH3T3 cells migration assay. This performance is less effective than the results observed in the current study for certain copper concentrations (Samples B, C, and D). Although the PVA/chitosan electrospun matrix in their study achieved a

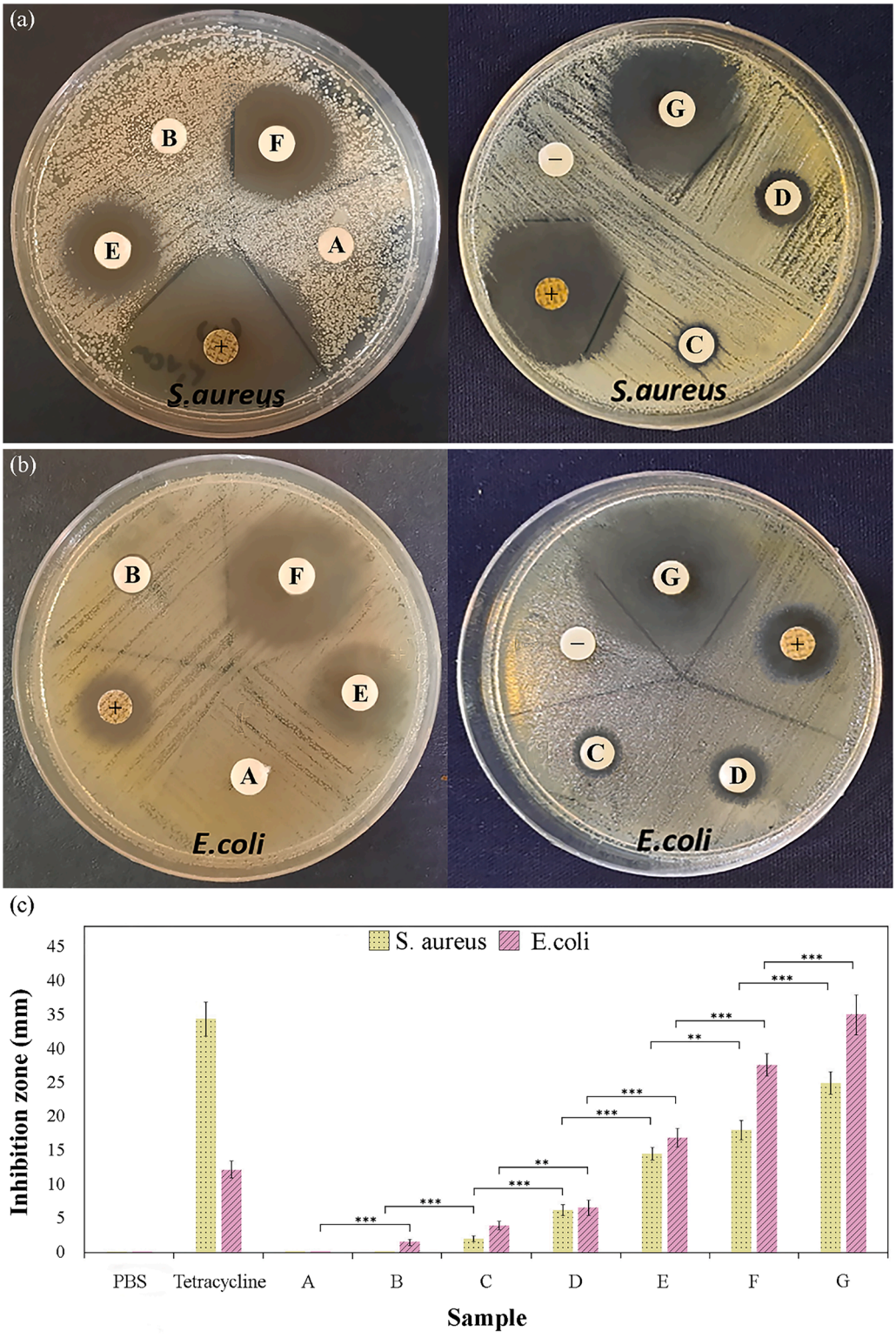

Fig. 9. Antibacterial disc diffusion results of the samples against S. aureus (a) and E. coli (b). Zones of inhibition associated with the samples against each bacterial strain (c), with**, and *** denoting statistically significant differences with $p < 0.01$, and $p < 0.001$, respectively.

uniform distribution of CuO nanoparticles, the complexation used in the present research in the same matrix demonstrates a superior release profile and wound closure potential. These findings provide further evidence supporting the superiority of complexation delivery systems over other incorporation methods for wound healing applications.

3.11. Antibacterial activity of wound dressings

The results obtained from the antibacterial disk diffusion assay (Fig. 9) demonstrate that the nanofibers composed of the chitosan-copper complex displayed varying levels of antibacterial efficacy. In the absence of copper ions, Sample A exhibited no antibacterial activity against either *S. aureus* or *E. coli*. Sample B, which had a copper amount of 1 %, exhibited little antibacterial activity. It demonstrated an inhibition zone of 1.6 ± 0.2 mm against *E. coli*, while no difference was observed against *S. aureus*. Sample C with 3 % copper has the minimum copper concentration which prevented the growth of both bacteria strains, *E. coli* by 4.0 ± 0.4 mm and *S. aureus* by 2.0 ± 0.3 mm. These results suggest that while chitosan alone does not exhibit any detectable antibacterial effect against *E. coli* and *S. aureus*, it acts synergistically when complexed with copper. This is because the minimum inhibitory concentration (MIC) identified in this study is lower than previously reported studies on copper's antibacterial properties (Ruparelia et al., 2008, Cioffi and Rai, 2012). Sample G which had the higher concentration of copper, led to a notable inhibition zone measuring 35.2 ± 2.9 mm against *E. coli* and 25.1 ± 1.6 mm against *S. aureus*. Khodabakhsh *et al.* (Eskandarinia et al., 2020) reported that inhibition zones of 5.4 mm against *S. aureus* and 1.9 mm against *E. coli* are noteworthy to support wound healing in vivo, which validates the antibacterial effectiveness of Sample D in the current study.

Copper is recognized for its strong antimicrobial properties, making it highly effective in various biomedical applications. Copper ions exhibit antibacterial activity against both gram-positive and gram-negative bacteria. Gram-negative bacteria, with their outer membrane of lipopolysaccharides (LPS) and porins, have higher susceptibility because copper ions bind to LPS, disrupt membrane integrity, and increase copper ion absorption (Godoy-Gallardo et al., 2021, Bhamidimarri et al., 2021). In contrast, gram-positive bacteria have a protective peptidoglycan layer and weaker interactions with copper ions, but copper still generates ROS, causing oxidative stress and damage. Additionally, copper's affinity for electron-rich molecules in the peptidoglycan layer enhances its penetration and potential to harm proteins and DNA (Godoy-Gallardo et al., 2021).

4. Conclusion

In this study, free-standing chitosan-copper complexes/PVA nanofibrous mats were successfully fabricated using electrospinning. The chemical coordination of copper binding in complexation facilitated a desired initial burst release of copper ions, followed by a controlled release over one week. This release kinetics offered an enhanced balance between cytotoxicity and antibacterial activity. The complexation of copper with chitosan also synergistically enhanced its antibacterial activity. Specifically, the sample containing 6 % copper relative to chitosan amine groups (Sample D) demonstrated the most promising potential for managing infected wounds, benefiting from an optimal balance of antibacterial activity, fibroblast cytocompatibility, and cell migration necessary for promoting wound closure. The lower toxicity, more readily metabolized nature, and ability of copper to promote wound healing and tissue regeneration—compared to silver used in commercially available antibiotic-free antibacterial wound dressings (such as Acticoat)—support the potential for the further development of chitosan-copper complex-based dressings. The straightforward production method and cost-effectiveness of the materials used in these constructs offer additional promising commercial prospects.

CRediT authorship contribution statement

Amir Parvinnasab: Writing – original draft, Visualization, Validation, Resources, Methodology, Investigation, Data curation. **Sharareh Shahroudi:** Writing – review & editing, Visualization, Validation, Resources, Methodology, Investigation, Data curation. **Erfan Salahinejad:** Writing – review & editing, Supervision, Conceptualization. **Amir Hossein Taghvaei:** Writing – review & editing, Resources, Conceptualization. **Seyed Adel Sharifi Fard:** Investigation. **Esmaeel Sharifi:** Writing – review & editing, Resources, Investigation.

Declaration of competing interest

The authors declare that they have no known competing financial interests or personal relationships that could have appeared to influence the work reported in this paper.

Data availability

Data will be made available on request.

References

Abbas, W. A., Sharafeldin, I. M., Omar, M. M., & Allam, N. K. (2020). Novel mineralized electrospun chitosan/PVA/TiO 2 nanofibrous composites for potential biomedical applications: Computational and experimental insights. *Nanoscale Advances, 2*(4), 1512–1522.

Abraham, A., Soloman, P., & Rejini, V. (2016). Preparation of chitosan-polyvinyl alcohol blends and studies on thermal and mechanical properties. *Procedia Technology, 24*, 741–748.

Abutaleb, A., Lolla, D., Aljuhani, A., Shin, H. U., Rajala, J. W., & Chase, G. G. (2017). Effects of surfactants on the morphology and properties of electrospun polyetherimide fibers. *Fibers, 5*(3), 33.

Akhtar, M. A., Ilyas, K., Dlouhý, I., Siska, F., & Boccaccini, A. R. (2020). Electrophoretic deposition of copper (II)–chitosan complexes for antibacterial coatings. *International Journal of Molecular Sciences, 21*(7), 2637.

Alturki, A. M. (2022). Facile synthesis route for chitosan nanoparticles doped with various concentrations of the biosynthesized copper oxide nanoparticles: Electrical conductivity and antibacterial properties. *Journal of Molecular Structure, 1263*, Article 133108.

Azizi Amirabad, A., Johari, M., Parichehr, R., Aghdam, R. M., Dehghanian, C., & Allahkaram, S. R. (2023). Improving corrosion, antibacterial and biocompatibility properties of MAO-coated AZ31 magnesium alloy by Cu (II)-chitosan/PVA nanofibers post-treatment. *Ceramics International, 49*(11), 17371–17382.

Barnes, C. P., Sell, S. A., Boland, E. D., Simpson, D. G., & Bowlin, G. L. (2007). Nanofiber technology: Designing the next generation of tissue engineering scaffolds. *Advanced Drug Delivery Reviews, 59*(14), 1413–1433.

Beam, J. W. (2007). Management of superficial to partial-thickness wounds. *Journal of Athletic Training, 42*(3), 422.

Bhamidimarri, S. P., Young, T. R., Shanmugam, M., Soderholm, S., Baslé, A., Bumann, D., et al. (2021). Acquisition of ionic copper by the bacterial outer membrane protein OprC through a novel binding site. *PLoS Biology, 19*(11), Article e3001446.

Caetano, G. F., Frade, M. A. C., Andrade, T. A. M., Leite, M. N., Bueno, C. Z., Moraes, Â. M., et al. (2015). Chitosan-alginate membranes accelerate wound healing. *Journal of Biomedical Materials Research Part B: Applied Biomaterials, 103*(5), 1013–1022.

Chen, S.-Y., Liu, S.-T., Lin, W.-R., Lin, C.-K., & Huang, S.-M. (2019). The mechanisms underlying the cytotoxic effects of copper via differentiated embryonic chondrocyte gene 1. *International Journal of Molecular Sciences, 20*(20), 5225.

N. Cioffi, M. Rai, Nano-antimicrobials: Progress and prospects, (2012).

Costa, C. N., Teixeira, V. G., Delpech, M. C., Souza, J. V. S., & Costa, M. A. (2015). Viscometric study of chitosan solutions in acetic acid/sodium acetate and acetic acid/sodium chloride. *Carbohydrate Polymers, 133*, 245–250.

Cui, W., Li, X., Zhou, S., & Weng, J. (2008). Degradation patterns and surface wettability of electrospun fibrous mats. *Polymer Degradation and Stability, 93*(3), 731–738.

Dash, P., Thirumurugan, S., Tseng, C.-L., Lin, Y.-C., Chen, S.-L., Dhawan, U., et al. (2023). Synthesis of methotrexate-loaded dumbbell-shaped titanium dioxide/gold nanorods coated with mesoporous silica and decorated with upconversion nanoparticles for near-infrared-driven trimodal cancer treatment. *ACS Applied Materials & Interfaces, 15*(28), 33335–33347.

Dzhardimalieva, G. I., Rabinskiy, L. N., Kydralieva, K. A., & Uflyand, I. E. (2019). Recent advances in metallopolymer-based drug delivery systems. *RSC Advances, 9*(63), 37009–37051.

Eskandarinia, A., Kefayat, A., Agheb, M., Rafienia, M., Amini Baghbadorani, M., Navid, S., et al. (2020). A novel bilayer wound dressing composed of a dense polyurethane/propolis membrane and a biodegradable polycaprolactone/gelatin nanofibrous scaffold. *Scientific Reports, 10*(1), 3063.

Farshi, P., Salarian, R., Rabiee, M., Alizadeh, S., Gholipourmalekabadi, M., Ahmadi, S., et al. (2022). Design, preparation, and characterization of silk fibroin/carboxymethyl cellulose wound dressing for skin tissue regeneration applications. *Polymer Engineering & Science, 62*(9), 2741–2749.
Feng, P., Luo, Y., Ke, C., Qiu, H., Wang, W., Zhu, Y., et al. (2021). Chitosan-based functional materials for skin wound repair: Mechanisms and applications. *Frontiers in Bioengineering and Biotechnology, 9*, Article 650598.
Feng, W., & Wang, Z. (2023). Tailoring the swelling-shrinkable behavior of hydrogels for biomedical applications. *Advanced Science, 10*(28), Article 2303326.
Feng, Y., Ming, T., Zhou, J., Lu, C., Wang, R., & Su, X. (2022). The response and survival mechanisms of Staphylococcus aureus under high salinity stress in salted foods. *Foods (Basel, Switzerland), 11*(10), 1503.
Gaetke, L. M., & Chow, C. K. (2003). Copper toxicity, oxidative stress, and antioxidant nutrients. *Toxicology, 189*(1–2), 147–163.
Garcia Garcia, C. E., Bossard, F., & Rinaudo, M. (2021). Electrospun biomaterials from chitosan blends applied as scaffold for tissue regeneration. *Polymers, 13*(7), 1037.
Gholivand, K., Mohammadpour, M., Derakhshankhah, H., Samadian, H., Aghaz, F., Malekshah, R. E., et al. (2023). Composites based on alginate containing formylphosphazene-crosslinked chitosan and its Cu (II) complex as an antibiotic-free antibacterial hydrogel dressing with enhanced cytocompatibility. *International Journal of Biological Macromolecules, 253*, Article 127297.
Godoy-Gallardo, M., Eckhard, U., Delgado, L. M., de Roo Puente, Y. J., Hoyos-Nogués, M., Gil, F. J., et al. (2021). Antibacterial approaches in tissue engineering using metal ions and nanoparticles: From mechanisms to applications. *Bioactive Materials, 6*(12), 4470–4490.
Gritsch, L., Lovell, C., Goldmann, W. H., & Boccaccini, A. R. (2018). Fabrication and characterization of copper (II)-chitosan complexes as antibiotic-free antibacterial biomaterial. *Carbohydrate Polymers, 179*, 370–378.
Guo, C., Cheng, F., Liang, G., Zhang, S., Jia, Q., He, L., et al. (2022). Copper-based polymer-metal–organic framework embedded with Ag nanoparticles: Long-acting and intelligent antibacterial activity and accelerated wound healing. *Chemical Engineering Journal, 435*, Article 134915.
Huang, C.-Y., Hu, K.-H., & Wei, Z.-H. (2016). Comparison of cell behavior on pva/pva-gelatin electrospun nanofibers with random and aligned configuration. *Scientific Reports, 6*(1), 37960.
Iqbal, H., Khan, B. A., Khan, Z. U., Razzaq, A., Khan, N. U., Menaa, B., et al. (2020). Fabrication, physical characterizations and in vitro antibacterial activity of cefadroxil-loaded chitosan/poly (vinyl alcohol) nanofibers against Staphylococcus aureus clinical isolates. *International Journal of Biological Macromolecules, 144*, 921–931.
Jayasekara, R., Harding, I., Bowater, I., & Lonergan, G. (2005). Biodegradability of a selected range of polymers and polymer blends and standard methods for assessment of biodegradation. *Journal of Polymers and the Environment, 13*, 231–251.
Kardos, J., Héja, L., Simon, Á., Jablonkai, I., Kovács, R., & Jemnitz, K. (2018). Copper signalling: Causes and consequences. *Cell Communication and Signaling, 16*, 1–22.
Kentish, S. E., Scholes, C. A., & Stevens, G. W. (2008). Carbon dioxide separation through polymeric membrane systems for flue gas applications. *Recent Patents on Chemical Engineering, 1*(1), 52–66.
Khan, M. N., Arafat, M. T., Rashid, T. U., Haque, P., & Rahman, M. M. (2024). Chitosan-stabilized CuO nanostructure-functionalized UV-crosslinked PVA/Chitosan electrospun membrane as enhanced wound dressing. *ACS Applied Bio Materials, 7*(2), 961–976.
Khil, M. S., Cha, D. I., Kim, H. Y., Kim, I. S., & Bhattarai, N. (2003). Electrospun nanofibrous polyurethane membrane as wound dressing. *Journal of Biomedical Materials Research Part B: Applied Biomaterials: An Official Journal of The Society for Biomaterials, The Japanese Society for Biomaterials, and The Australian Society for Biomaterials and the Korean Society for Biomaterials, 67*(2), 675–679.
Kim, H., Panda, P. K., Sadeghi, K., & Seo, J. (2023). Poly (vinyl alcohol)/hydrothermally treated tannic acid composite films as sustainable antioxidant and barrier packaging materials. *Progress in Organic Coatings, 174*, Article 107305.
Kong, M., Chen, X. G., Xing, K., & Park, H. J. (2010). Antimicrobial properties of chitosan and mode of action: A state of the art review. *International Journal of Food Microbiology, 144*(1), 51–63.
Koosha, M., & Mirzadeh, H. (2015). Electrospinning, mechanical properties, and cell behavior study of chitosan/PVA nanofibers. *Journal of Biomedical Materials Research Part A, 103*(9), 3081–3093.
Letelier, M. E., Lepe, A. M., Faúndez, M., Salazar, J., Marín, R., Aracena, P., et al. (2005). Possible mechanisms underlying copper-induced damage in biological membranes leading to cellular toxicity. *Chemico-Biological Interactions, 151*(2), 71–82.
Letelier, M. E., Sánchez-Jofré, S., Peredo-Silva, L., Cortés-Troncoso, J., & Aracena-Parks, P. (2010). Mechanisms underlying iron and copper ions toxicity in biological systems: Pro-oxidant activity and protein-binding effects. *Chemico-Biological Interactions, 188*(1), 220–227.
Li, J., & Zhuang, S. (2020). Antibacterial activity of chitosan and its derivatives and their interaction mechanism with bacteria: Current state and perspectives. *European Polymer Journal, 138*, Article 109984.
Li, S., Xie, H., Li, S., & Kang, Y. J. (2012). Copper stimulates growth of human umbilical vein endothelial cells in a vascular endothelial growth factor-independent pathway. *Experimental Biology and Medicine, 237*(1), 77–82.
Lončarević, A., Ivanković, M., & Rogina, A. (2021). Electrosprayed chitosan–copper complex microspheres with uniform size. *Materials, 14*(19), 5630.
Maquart, F., & Monboisse, J. (2014). Extracellular matrix and wound healing. *Pathologie Biologie, 62*(2), 91–95.
Mekahlia, S., & Bouzid, B. (2009). Chitosan-Copper (II) complex as antibacterial agent: Synthesis, characterization and coordinating bond-activity correlation study. *Physics Procedia, 2*(3), 1045–1053.
Mroczek-Sosnowska, N., Sawosz, E., Vadalasetty, K. P., Łukasiewicz, M., Niemiec, J., Wierzbicki, M., et al. (2015). Nanoparticles of copper stimulate angiogenesis at systemic and molecular level. *International Journal of Molecular Sciences, 16*(3), 4838–4849.
Nikonenko, N., Buslov, D., Sushko, N., & Zhbankov, R. (2005). Spectroscopic manifestation of stretching vibrations of glycosidic linkage in polysaccharides. *Journal of Molecular Structure, 752*(1–3), 20–24.
Olvera Bernal, R. A., Olekhnovich, R. O., & Uspenskaya, M. V. (2023). Chitosan/PVA nanofibers as potential material for the development of soft actuators. *Polymers, 15*(9), 2037.
Paluszkiewicz, C., Stodolak, E., Hasik, M., & Blazewicz, M. (2011). FT-IR study of montmorillonite–chitosan nanocomposite materials. *Spectrochimica Acta Part A: Molecular and Biomolecular Spectroscopy, 79*(4), 784–788.
Panda, P. K., Park, K., & Seo, J. (2023). Development of poly (vinyl alcohol)/regenerated chitosan blend film with superior barrier, antioxidant, and antibacterial properties. *Progress in Organic Coatings, 183*, Article 107749.
Percival, N. J. (2002). Classification of wounds and their management. *Surgery (Oxford), 20*(5), 114–117.
Pestov, A., & Bratskaya, S. (2016). Chitosan and its derivatives as highly efficient polymer ligands. *Molecules (Basel, Switzerland), 21*(3), 330.
Rabea, E. I., Badawy, M. E.-T., Stevens, C. V., Smagghe, G., & Steurbaut, W. (2003). Chitosan as antimicrobial agent: Applications and mode of action. *Biomacromolecules, 4*(6), 1457–1465.
Rácová, Z., Ryparová, P., Hlaváč, R., Tesárek, P., & Nežerka, V. (2014). Influence of copper ions on mechanical properties of PVA-based nanofiber textiles. *Applied Mechanics and Materials, 486*, 201–204.
Rahmati, M., Mills, D. K., Urbanska, A. M., Saeb, M. R., Venugopal, J. R., Ramakrishna, S., et al. (2021). Electrospinning for tissue engineering applications. *Progress in Materials Science, 117*, Article 100721.
Rashid, M., Rabbi, M. A., Ara, T., Hossain, M. M., Islam, M. S., Elaissari, A., et al. (2021). Vancomycin conjugated iron oxide nanoparticles for magnetic targeting and efficient capture of Gram-positive and Gram-negative bacteria. *RSC Advances, 11*(57), 36319–36328.
Rhazi, M., Desbrieres, J., Tolaimate, A., Rinaudo, M., Vottero, P., & Alagui, A. (2002). Contribution to the study of the complexation of copper by chitosan and oligomers. *Polymer, 43*(4), 1267–1276.
Rohyami, Y., & Sari, N. A. (2021). Simple method on determination of deacetyllation degree for chitosan. *AIP Conference Proceedings*.
Ruparelia, J. P., Chatterjee, A. K., Duttagupta, S. P., & Mukherji, S. (2008). Strain specificity in antimicrobial activity of silver and copper nanoparticles. *Acta Biomaterialia, 4*(3), 707–716.
Safdar, R., Omar, A. A., Arunagiri, A., Regupathi, I., & Thanabalan, M. (2019). Potential of Chitosan and its derivatives for controlled drug release applications–A review. *Journal of Drug Delivery Science and Technology, 49*, 642–659.
Sánchez-Machado, D. I., López-Cervantes, J., Escárcega-Galaz, A. A., Campas-Baypoli, O. N., Martínez-Ibarra, D. M., & Rascón-León, S. (2024). Measurement of the degree of deacetylation in chitosan films by FTIR, 1H NMR and UV spectrophotometry. *MethodsX, 12*, Article 102583.
Sandra, S., Anakha, D., Silpa, C., Vyshnavi, T., Bhagiyalakshmi, M., Yamuna, R., et al. (2024). Synthesis of electrospun PVA/chitosan nanofibrous scaffold impregnated with CuO nanoparticles for wound healing. *Cellulose (London, England)*, 1–15.
Sencadas, N., Diez-Perez, A., Ribelles, J. G., & Lanceros-Méndez, S. (2017). 5. Influence of crystallinity on hydrophobicity and biological response of poly (L-lactide) electrospun mats. *Escola de Ciències*, 79.
Sportelli, M. C., Volpe, A., Picca, R. A., Trapani, A., Palazzo, C., Ancona, A., et al. (2016). Spectroscopic characterization of copper-chitosan nanoantimicrobials prepared by laser ablation synthesis in aqueous solutions. *Nanomaterials, 7*(1), 6.
Tabesh, E., Salimijazi, H., Kharaziha, M., & Hejazi, M. (2018). Antibacterial chitosan-copper nanocomposite coatings for biomedical applications. *Materials Today: Proceedings, 5*(7), 15806–15812.
Turishchev, S. Y., Marchenko, D., Sivakov, V., Belikov, E., Chuvenkova, O., Parinova, E., et al. (2020). On the possibility of photoemission electron microscopy for E. coli advanced studies. *Results in Physics, 16*, Article 102821.
Verlee, A., Mincke, S., & Stevens, C. V. (2017). Recent developments in antibacterial and antifungal chitosan and its derivatives. *Carbohydrate Polymers, 164*, 268–283.
Vijayan, A., Nanditha, C., & Kumar, G. V. (2021). ECM-mimicking nanofibrous scaffold enriched with dual growth factor carrying nanoparticles for diabetic wound healing. *Nanoscale Advances, 3*(11), 3085–3092.
Xiao, J., Chen, S., Yi, J., Zhang, H. F., & Ameer, G. A. (2017). A cooperative copper metal–organic framework-hydrogel system improves wound healing in diabetes. *Advanced Functional Materials, 27*(1), Article 1604872.
Yang, J. M., Panda, P. K., Jie, C. J., Dash, P., & Chang, Y. H. (2022). Poly (vinyl alcohol)/chitosan/sodium alginate composite blended membrane: Preparation, characterization, and water-induced shape memory phenomenon. *Polymer Engineering & Science, 62*(5), 1526–1537.
Yilmaz Atay, H. (2019). Antibacterial activity of chitosan-based systems. *Functional Chitosan: Drug Delivery and Biomedical Applications*, 457–489.

Young, J. L., Holle, A. W., & Spatz, J. P. (2016). Nanoscale and mechanical properties of the physiological cell–ECM microenvironment. *Experimental Cell Research, 343*(1), 3–6.

Zafari, M., Mansouri, M., Omidghaemi, S., Yazdani, A., Pourmotabed, S., Hasanpour Dehkordi, A., et al. (2020). Physical and biological properties of blend-electrospun polycaprolactone/chitosan-based wound dressings loaded with N-decyl-N, N-dimethyl-1-decanaminium chloride: An in vitro and in vivo study. *Journal of Biomedical Materials Research Part B: Applied Biomaterials, 108*(8), 3084–3098.

Zhang, C., Li, Y., Wang, P., Li, J., Weiss, J., & Zhang, H. (2020). Core-shell nanofibers electrospun from O/W emulsions stabilized by the mixed monolayer of gelatin-gum Arabic complexes. *Food Hydrocolloids, 107*, Article 105980.